Contemporary Mathematics
https://ojs.wiserpub.com/index.php/CM/

Research Article

Enhanced Frequency Control in Power Systems Using a Novel Meerkat Optimization Algorithm

Yousefali Javanighadikolaei, Mohammad Tolou Askari*, Meysam Amirahmadi, Majid Babaeinik

Department of Electrical Engineering, Semnan Branch, Islamic Azad University, Semnan, Iran
E-mail: m.askari@semnaniau.ac.ir

Received: 10 December 2024; **Revised:** 10 February 2025; **Accepted:** 19 February 2025

Abstract: Frequency regulation in power systems remains a significant challenge due to inherent nonlinearities and dynamic load variations. This paper introduces a novel adaptive control strategy that integrates state feedback with the Meerkat Optimization Algorithm (MOA) to enhance frequency stability and minimize power imbalances. The proposed approach explicitly incorporates nonlinear constraints-such as governor saturation and power quality disturbances-within a multi-objective optimization framework to strategically position the closed-loop system poles for improved transient response and robustness. Furthermore, fuzzy logic is integrated into the MOA to dynamically tune control parameters in real time, thereby addressing system parameter variations and operational constraints. Numerical simulations on both a two-area power system with nonlinear governor constraints and the New England 39-bus test system demonstrate that the proposed MOA-based controller significantly outperforms conventional Proportional-Integral (PI) controllers as well as other recent optimization methods. Notable improvements include reductions in settling time and peak overshoot of up to 35% and 20%, respectively, underscoring the efficacy of the proposed approach in achieving superior frequency regulation under realistic operating conditions.

***Keywords*:** frequency control, meerkat optimization algorithm, mode feedback controller, virtual controller design

MSC: 65L05, 34K06, 34K28

Abbreviation

MOA	Meerkat Optimization Algorithm
PI	Proportional-Integral
ΔP_{21}	Power deviation between areas 2 and 1
$\Delta\omega_2$	Frequency deviation in area 2
ACE_2	Area control error in zone 2
J_c	Cost function
X_{it}	Position of the ith meerkat at time t
X_{jt}	Position of a randomly chosen meerkat at time t
rand	Random value between 0 and 1

DOI: https://doi.org/10.37256/cm.6320256227

step	Step size
X_{gbt}	Global best position at time t
Xemergencyt	Emergency position at time t
div	Diversification parameter
ΔP_{ref1}	Reference power change in area 1
ΔP_{ref2}	Reference power change in area 2
ΔP_{v1}	Power variation in area 1
ΔP_{m1}	Mechanical power variation in area 1
ΔP_{tie}	Power tie-line deviation
ΔP_{v2}	Power variation in area 2
ΔP_{m2}	Mechanical power variation in area 2
ΔA_1	Area error in area 1
ΔA_2	Area error in area 2
α_v	Parameter related to the Levy distribution
ub	Upper bound
lb	Lower bound

1. Introduction

In contemporary times, as power systems grow in scale and intricacy, there arises a pressing necessity to cater to a diverse array of small and large consumption loads. These loads span various sectors, encompassing residential, commercial, and industrial domains. Consequently, the focus shifts towards ensuring the reliability and robust stability of the power grid amidst both internal dynamics and external perturbations. The significance has escalated. Among the paramount attributes governing power system functionality lies the stability of system frequency, denoting minimal deviations within acceptable margins. Put differently, maintaining a steady frequency within defined bounds is imperative for optimizing power system performance. Preserving frequency at its nominal value guarantees consistent operation speeds for both induction and synchronous motors. This consistency holds particular significance for gas, hydroelectric, and combined-cycle power facilities. Moreover, within a network, a substantial frequency decline induces robust magnetic currents in induction motors and transformers [1]. The equilibrium of active power generation and consumption dictates frequency stability within a power grid. Given the pervasive nature of frequency across the system, alterations in active power demand at any given point manifest as frequency fluctuations throughout the grid. Moreover, within interconnected power systems comprising multiple distinct control zones, maintaining prescribed power transmission levels between neighboring regions is imperative alongside individual zone frequency regulation [2]. The automated control mechanism, tasked with rectifying discrepancies between consumption and production by adjusting generator output, thereby maintaining nominal values for frequency and transmission power in the lines, is Load Frequency Control (LFC) or Automatic Generation Control (AGC). Within power systems, the primary objective of frequency load control is twofold: mitigating frequency deviations and regulating power interchange between regions to minimize network inefficiencies [3].

1.1 *Motivation*

The motivation for this research is driven by the critical need to enhance Load Frequency Control (LFC) in power systems, which is a fundamental aspect of ensuring reliable and efficient grid operation. Traditional LFC methods, such as Proportional-Integral (PI) controllers, often fall short in addressing the complex dynamics and nonlinearities present in modern power systems. These systems are increasingly integrated with renewable energy sources and subjected to varying load demands, leading to more frequent and severe disturbances. One of the primary challenges is dealing with nonlinear constraints. Traditional control methods typically assume linear models for power systems. However, real-world power systems exhibit significant nonlinearities, such as governor saturation and production constraints. These nonlinearities

can lead to suboptimal performance of the control systems and increased susceptibility to disturbances. Addressing these nonlinearities is crucial for improving the robustness and efficiency of LFC. Another challenge is the use of fixed gain parameters in classical PI controllers. These controllers operate with fixed gain parameters, which are usually tuned for nominal conditions. This fixed tuning does not adapt well to variations in system parameters and operational conditions, resulting in degraded performance under different scenarios. There is a need for control strategies that can dynamically adjust to changing conditions. Ensuring system stability while optimizing performance attributes such as settling time and peak response time is a significant challenge. The ability to maintain frequency stability within predefined bounds is essential for the optimal functioning of power systems, particularly in the presence of high penetration of renewable energy sources. The development and integration of advanced optimization algorithms, like the Meerkat Optimization Algorithm (MOA), into LFC is relatively new. While these algorithms offer potential improvements in solving complex optimization problems, their practical implementation and effectiveness in real-world power systems need thorough investigation and validation. The research addresses these obstacles by introducing an innovative method that combines state feedback control with the Meerkat Optimization Algorithm (MOA), improved through the application of fuzzy logic. The objectives include developing a robust control strategy that effectively handles nonlinear constraints, designing a dynamic control system capable of adapting to varying operational conditions, and demonstrating the superiority of the proposed method through numerical simulations and comparative analysis with traditional PI controllers.

1.2 *Literature review*

In [1] Power System Stability and Control provides comprehensive insights into the principles and challenges of maintaining power system stability, while in [2] a survey of Load Frequency Control (LFC) strategies outlines the evolution of these techniques and identifies gaps for future research. In [3] an extended integral control approach is proposed that incorporates generation-rate constraints to improve system performance, and in [4] adaptive fuzzy gain scheduling for LFC is explored to enhance dynamic response by adjusting controller gains in real time. In [5] robust automatic generation control methods are introduced to maintain stability amid uncertainties, and in [6] robust control design using μ-synthesis is presented to address inaccuracies in system models and external disturbances. In [7] a robust Proportional-Integral-Derivative Control (PID) controller specifically tailored for LFC is developed, while in [8] modified dynamic neural networks are applied to capture the nonlinear behavior of modern power systems. In [9] artificial neural networks are used for load modeling to improve the accuracy and performance of LFC systems, and in [10] a multi-stage fuzzy PID controller for automatic generation control in deregulated environments is designed. In [11] an optimal fuzzy logic-based PID controller that includes superconducting magnetic energy storage units is proposed to significantly enhance frequency stability, and in [12] Particle Swarm Optimization (PSO) is employed to adjust PID controller settings for multi-area LFC. In [13] decentralized LFC using hybrid PSO algorithms in deregulated power systems is investigated, and in [14] the Teaching-learning-based optimization method is introduced for constrained mechanical design problems with applications in LFC. In [15] the optimal design and real-time implementation of autonomous microgrids are discussed, focusing on active load management to enhance performance and reliability, while in [16] a method is presented for investing in batteries alongside fossil resources to reduce network costs. In [17] the economical and reliable operation of microgrids through hierarchical control is examined, and in [18] hierarchical control strategies are explored for the economic operation and resilience enhancement of DC microgrids. In [19] robust energy management and economic analysis of microgrids are conducted considering different battery characteristics, and in [20] the Meerkat Optimization Algorithm (MOA) is introduced as a new meta-heuristic for solving constrained engineering problems, demonstrating its potential in optimizing LFC systems. In [21] proactive stabilization of grid faults in DFIG-based wind farms is studied using bridge-type fault current limiters and nonlinear model predictive control, while in [22] the role of variable speed wind turbine generators in frequency regulation is analyzed through Active Disturbance Rejection Control (ADRC) and Reference, Setpoint, Tracking (RST) controllers. In [23] a hybrid evaluation methodology for generation technologies in hybrid microgrids is introduced, and in [24] a comparative techno-economic analysis of hybrid microgrids across diverse climatic regions is conducted. In [25] the optimal design of microgrids for resilient distribution networks is explored, and in [26] evolutionary algorithms combined with energy storage are applied to manage power and energy in low-voltage microgrids. In [27] distributed control and communication methods within networked microgrids are reviewed, while in

[28] home energy management systems are addressed with discussions on storage, Photovoltaic (PV), demand pricing, and electric vehicle scheduling. In [29] an innovative power management strategy for hybrid renewable energy systems that incorporates electric vehicles is proposed, and in [30] intelligent frequency control in AC microgrids using an online PSO-based fuzzy tuning method is demonstrated. In [31] a unique approach that combines an electrolyzer system with a fuzzy PI controller for frequency regulation in microgrid power systems is discussed, and in [32] state feedback combined with integral control is used for maintaining frequency stability in microgrids. In [33] the role of variable-speed wind energy conversion systems in frequency regulation is elaborated, and in [34] wind turbines emulating inertia for primary frequency control are examined. In [35] the dynamics of doubly fed induction generators in multi-area LFC are analyzed, and in [36] a sustainable large storage model for substations connected to the transmission grid is proposed. In [37] differential evolution-based robust LFC for microgrids equipped with energy storage systems is explored, and in [38] the control of greenhouse gas emissions through optimized DER technology investment and energy management in zero-net-energy buildings is examined. In [39] optimal frequency control for AC-network-based virtual generators is proposed using adaptive dynamic programming, and in [40] a generic model that considers operating limitations, production, and reconfiguration in the power grid is provided. In [41] centralized model forecasting control is suggested for transient frequency control in island-based inverters, and in [42] the transient synchronization stability of an islanded AC microgrid is examined with consideration of grid-forming and grid-following converter interactions. In [43] a systematic controller design for inverter-based microgrids with large signal stability and absorption range is presented, while in [44] major issues and challenges in microgrid modeling for stability analysis are discussed. In [45] a large signal stability analysis based on a T-S phase model of DC microgrids with different loads is developed, and in [46] a method to ensure transient stability with a guaranteed absorption area in DC microgrids is presented. In [47] a single-phase community microgrid model and its sustainability challenges are described, and in [48] the flexibility and stability of distributed secondary controllers in DC microgrids under cyber-attacks and communication delays are analyzed. In [49] transient stability analysis of microgrids considering the effect of the current controller of the downstream converter is proposed, and in [50] an improved Lyapunov neural method is presented to evaluate the transient stability of meshed microgrids.

1.3 *Contribution and research gap*

A thorough review of the existing literature on Load Frequency Control (LFC) in power systems reveals several key gaps that remain unaddressed in Table 1:

1. **Limited consideration of nonlinear constraints:** Most existing studies focus on linear models of power systems, which fail to capture real-world nonlinearities such as governor saturation, generation rate limits, and reactive power fluctuations. These constraints have a significant impact on system stability but are often ignored in optimization-based LFC approaches.

2. **Lack of dynamic and adaptive control strategies:** Traditional PI controllers and even some advanced metaheuristic-based methods use fixed or pre-tuned control gains, which do not adapt to changing system conditions. This limits their effectiveness in handling load fluctuations and disturbances dynamically.

3. **Limited integration of metaheuristic optimization and fuzzy logic:** While fuzzy logic has been separately used to improve adaptability, there is a lack of research on its integration with metaheuristic algorithms for real-time tuning of control parameters, which could significantly enhance performance.

4. **Insufficient multi-objective optimization approaches:** Many studies focus solely on minimizing frequency deviation, without jointly optimizing other critical factors such as power transfer efficiency, transient response speed, and control effort. A comprehensive multi-objective approach is necessary for improved real-world applicability.

5. **Lack of comparative analysis with emerging optimization algorithms:** Recent studies have introduced novel algorithms such as the Mountain Gazelle Optimizer (MGO), Sunflower Optimization Algorithm (SFO), and Grey Wolf Optimizer (GWO) for LFC applications. However, a detailed comparison of their performance against new optimization techniques like the Meerkat Optimization Algorithm (MOA) remains unexplored.

Table 1. Comparison of this study with other previous studies

Article reference	Optimization algorithm/ controller	Methodology	Objective functions	Main contributions	Nonlinear constraints	Application
[1]	PSO-based fuzzy tuning	Online tuning approach for frequency control in AC microgrids	Frequency stability	Fuzzy logic tuning for better frequency control	Not discussed	AC microgrid
[2]	Fuzzy PI controller	Combines electrolyzer system for frequency control	Frequency response	Integration of electrolyzer with fuzzy PI controller	Not discussed	Microgrid with electrolyzer
[3]	State feedback with integral control	Uses state feedback with integral control for frequency regulation	Frequency regulation	Improved frequency control in microgrids	Not mentioned	Microgrid
[4]	Variable-speed wind energy system	Variable-speed wind turbine for frequency regulation	Frequency regulation	Uses wind turbines for supporting frequency control	Not discussed	Wind energy
[5]	Wind turbine emulating inertia	Wind turbines provide inertia for frequency support	Primary frequency control	Wind turbines supporting primary frequency control	Not mentioned	Wind energy
[6]	Doubly Fed Induction Generator (DFIG)	DFIG for load frequency control in multi-area systems	Load frequency control	DFIG contributes to multi-area load frequency control	Not discussed	Multi-area system
[7]	Back-to-Back converters	Energy distribution in microgrids with back-to-back converters	Energy distribution	Microgrid configuration for renewable power distribution	Not discussed	Microgrid
[8]	Differential evolution-based control	Energy storage system integrated for robust frequency control	Load frequency control	Robust control of microgrid with energy storage system	Not mentioned	Microgrid with energy storage
[9]	Optimal DER investment	Optimization of distributed energy resources (DER)	Emissions control	Controls emissions in zero-net-energy buildings	Not discussed	Zero-Net-Energy buildings
[10]	Adaptive dynamic programming	Virtual synchronous generator for frequency control	Frequency control	Adaptive dynamic programming for AC microgrids	Not discussed	AC microgrids
[11]	Inertia and resource adequacy planning	Inertia and resource planning for power systems	Inertia and resource adequacy	Planning for renewable-rich power systems	Not discussed	Renewable-rich power systems
[12]	Centralized model predictive control	Frequency control in inverter-based microgrids	Transient frequency control	Centralized predictive control for islanded microgrids	Not discussed	Inverter-based microgrids
[13]	Grid-forming and grid-following converters	Transient synchronization stability in AC microgrids	Transient synchronization stability	Interactions between grid-forming and grid-following converters	Considered	AC microgrid
[14]	Systematic controller design	Large-signal stability in inverter-based microgrids	Large-signal stability	Certified large-signal stability in microgrids	Not discussed	Inverter-based microgrids
[15]	Stability analysis	Microgrid modeling for stability analysis	Stability analysis	Microgrid modeling to enhance stability	Not discussed	Microgrid
[16]	T-S fuzzy model	Large-signal stability analysis for DC microgrids	Large-signal stability	Fuzzy model for large-signal stability analysis	Considered	DC microgrid

Table 1. (Cont.)

Article reference	Optimization algorithm/ controller	Methodology	Objective functions	Main contributions	Nonlinear constraints	Application
[17]	Neural lyapunov method	Transient stability assessment in DC microgrids	Transient stability	Ensures transient stability with guaranteed region of attraction	Considered	DC microgrid
[18]	Robust controller	Stability improvement for community microgrids	Stability improvement	Robust controller for islanded mode stability	Not discussed	Community microgrid
[19]	Distributed secondary controllers	Resilience and stability under cyber-attacks and delays	Resilience, stability	Resilience analysis under cyber-attacks	Not discussed	DC microgrids
[20]	Grid-following converter	Transient stability analysis for grid-following converters	Transient stability	Analyzes impact of current controllers on transient stability	Not discussed	Microgrid
[21]	Neural lyapunov method	Transient stability assessment using neural methods	Transient stability	Improved neural lyapunov method for stability assessment	Considered	Networked microgrids
This study	Meerkat optimization algorithm (MOA)	Multi-faceted cost function with pole placement and fuzzy logic	Frequency stability, power transmission	Nonlinear constraint handling with MOA	Considered	Two-zone power system with nonlinear constraints

To bridge these gaps, this study introduces a novel state feedback controller design based on the Meerkat Optimization Algorithm (MOA). The key contributions of this research are:

1. **Explicit consideration of nonlinear constraints:** The proposed method incorporates governor saturation and power quality constraints, providing a more realistic and robust control approach.

2. **Development of an adaptive MOA-based controller:** The novel MOA-based controller dynamically adjusts state feedback parameters, ensuring real-time adaptation to system changes.

3. **Integration of fuzzy logic with MOA:** The combination of fuzzy logic with MOA enables intelligent parameter tuning, improving stability and response speed.

4. **Implementation of a multi-objective optimization framework:** Unlike previous studies, this research jointly optimizes frequency deviation, settling time, power transfer efficiency, and transient response.

5. **Comparative performance evaluation against recent algorithms:** The effectiveness of the proposed MOA-based controller is validated through comparisons with recent methods, including MGO, SFO, and GWO, demonstrating its superiority.

By addressing these research gaps, this study provides a robust and adaptive solution for frequency regulation in power systems, offering significant advancements over existing methodologies. The results confirm that the proposed MOA-based approach effectively improves dynamic response, reduces frequency deviations, and enhances system resilience under uncertain operating conditions.

1.4 *Research organization*

The subsequent section of the manuscript offers a comprehensive yet succinct overview of the MOA algorithm. Following this, the third segment presents the structural framework of a two-zone power system incorporating Governor's saturation constraints. In the subsequent section, the methodology for devising an optimal state feedback controller utilizing the MOA algorithm is elucidated. Additionally, findings from simulations and numerical investigations on the

exemplar power system are detailed in the fifth segment. Lastly, the sixth section is dedicated to delivering the conclusive remarks of the paper. Figure 1 shows flowchart of the proposed approach in this article.

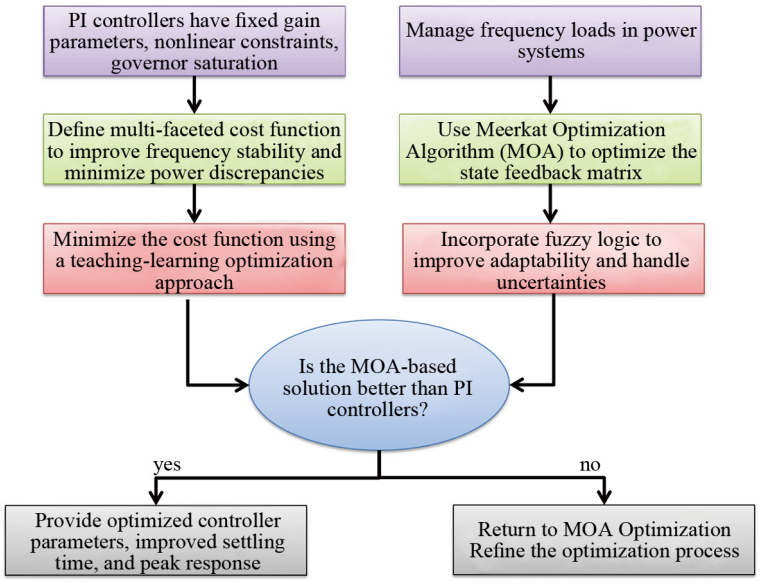

Figure 1. The flowchart of the proposed approach

2. The meerkat optimization algorithm (MOA)

The Meerkat Optimization Algorithm (MOA) is inspired by the social behavior of meerkats, a small mammal native to the deserts and plains of southern Africa. Known for their highly organized group behavior, meerkats live in large colonies and exhibit fascinating cooperative actions. These animals are particularly notable for their vigilance in detecting threats, which is a crucial part of their survival strategy. They take turns standing guard, with one individual serving as the "sentry" while the rest of the group forages or hunts. This behavior can be likened to the search for an optimal solution in an optimization problem, where the "sentry" helps the group avoid local traps and directs them towards promising areas in the search space.

Meerkats also exhibit a strong sense of collaboration. During foraging, they spread out to maximize their chances of finding food, and when a threat is detected, they quickly regroup, using social signals to coordinate their actions. This collaborative dynamic and the search for resources are the foundational principles behind MOA. The algorithm mimics these behaviors to explore and exploit the search space in a way that balances exploration (wide-ranging search) and exploitation (focused search on promising areas).

2.1 *Inspiration*

The meerkat, a small mammal with a distinctive brown striped coat, serves as an iconic representation of its species. This fascinating animal is typically found in desert areas or on expansive open plains. Being diurnal, the meerkat has a slender, elongated body and a long, thin tail that plays an essential role in helping it stand upright, acting as a stabilizer for balance. One striking feature of meerkats is the dark rings around their eyes, which function similarly to sunglasses, allowing them to see clearly even in bright sunlight. This unique adaptation enables them to gaze directly at the sun without strain, helping them detect potential threats from above. This trait is particularly beneficial in spotting predators that use the sun as camouflage. Drawing inspiration from the behavioral characteristics of meerkats, the Meerkat Optimization Algorithm (MOA) has been developed [51]. The following sections delve into the principles of MOA using a mathematical approach.

2.2 *Formation of the starting populations*

Meerkats naturally live in groups, displaying strong social tendencies. Likewise, the MOA initializes its population, X, using a specific equation that relies on a normal distribution within defined boundaries (ub and lb). This approach ensures that the population is distributed within the search space, resembling the spatial arrangement of meerkat colonies.

$$X = [X_1\, X_2\, \ldots\, X_i \ldots\, X_N] = \begin{bmatrix} X_{1,\,1} & X_{1,\,2} & \cdots & X_{1,\,j} & \cdots & X_{1,\,D} \\ X_{2,\,1} & X_{2,\,2} & \cdots & X_{2,\,j} & \cdots & X_{2,\,D} \\ \vdots & \vdots & \ddots & \vdots & \ddots & \vdots \\ X_{i,\,2} & X_{i,\,2} & \cdots & X_{i,\,j} & \cdots & X_{i,\,D} \\ \vdots & \vdots & \ddots & \vdots & \ddots & \vdots \\ X_{N,\,1} & X_{N,\,2} & \cdots & X_{N,\,j} & \cdots & X_{N,\,D} \end{bmatrix} \tag{1}$$

In this context, X_i denotes the solution being evaluated in the current iteration, forming the essence of the process. The population size is indicated by N, while D reflects the problem's dimensionality.

$$X_i^t = \text{random}_{\text{normal}}\,(\text{loc} = 0.5,\ \text{scale} = 0.3) \cdot (ub - lb) + lb \tag{2}$$

In this context, $\text{random}_{\text{normal}}$ refers to a number that is generated based on a normal distribution, representing natural fluctuations. This distribution is characterized by a fixed standard deviation of 0.3, which controls the level of variability and diversity in these random values. The presence of these random factors is essential in shaping the complexity and uncertainty within the MOA.

2.3 *Monitoring and tracking movements during predatory actions*

Meerkats adjust their behavior based on perceived threats, especially from predators and alert signals. If conditions appear safe-determined by a randomly assigned value under a set threshold (0.3)-they engage in either foraging or hunting with equal likelihood. This balanced approach enhances resource exploration through coordinated strategies.

$$\text{direct} = X_i^0 \tag{3}$$

$$\text{step} = \left(1 - {}^{\text{t}}/_{\text{T}}\right) r \tag{4}$$

$$X_i^{t+1} = X_i^t + \text{step} \cdot \text{direct} \tag{5}$$

when the symbolic variable P is below a defined threshold (rand), meerkats initiate their search by dispersing from a starting point called Direct. Their main objectives in this stage are locating food and staying alert to threats. The typical value of P is 0.5, maintaining a balance between these behaviors. The step size, which determines movement increments, decreases progressively with each iteration. This adaptive step influences both the extensive search phase and the final convergence, playing a crucial role in the algorithm's exploration and optimization process.

$$X_i^{t+1} = X_i^t + \text{step} \cdot \left(X_j^t - (\text{rand} + 0.5) \cdot X_i^t\right) \tag{6}$$

A meerkat sets out on an adventure filled with surprising encounters with its peers. As it navigates this experience, it seeks out and engages with others to collaborate on hunting activities. Here, X_j denotes a randomly selected meerkat from the group, different from the one initiating contact. This cooperative effort showcases the social nature of meerkats, emphasizing the role of teamwork in securing food.

2.4 *Escape or confront the adversary*

When a certain threshold, known as the sentry, is surpassed, meerkats become highly alert to potential dangers. They take on a watchful role, scanning their environment for predators or other hazards. If a threat is detected, they promptly alert their group, allowing each member to decide whether to seek shelter or stand their ground in defense.

$$\text{div} = \text{rand} + 0.1 \tag{7}$$

$$X^t_{\text{emergency}} = X^t_i + \left(2 \cdot \text{rand} \cdot X^t_{gb} - X^t_i\right) \tag{8}$$

$$X^{t+1}_i = X^t_{\text{emergency}}. \tag{9}$$

In urgent scenarios, meerkats assess their fitness using a specific criterion, $f\left(X^t_{\text{emergency}}\right)$. If this value surpasses another fitness measure, $f\left(X^t_i\right)$, the superior meerkat becomes the focal point, guiding the group. Its position serves as an optimal reference, influencing others to adjust their locations accordingly, as shown in Equation (8). This movement strategy mimics a defensive tactic where meerkats collectively appear larger to deter threats and protect the group.

$$X^{t+1}_i = \text{div} \cdot X^t_i - \left(2 * \text{rand} \cdot X^t_{gb} - X^t_i\right) \tag{10}$$

when the fitness function $f\left(X^t_{\text{emergency}}\right)$ meets or exceeds $f\left(X^t_i\right)$, meerkats show reduced tendency to follow their leader. This situation reflects the meerkats' recognition of incompatibility with the leader's path, particularly when they encounter barriers or threats that hinder their movement, or when facing opponents with greater strength. As a result, meerkats exhibit a behavior focused on survival, retreating away from the leader in search of safety and refuge, as detailed in Equation (10). The variable *div*, as presented in Equation (7), introduces an element of randomness designed to expand the exploratory behavior of individual meerkats, thus improving their ability to adapt within the search environment. Importantly, the variable *div* is not included in the leader's directional update, which is a strategic choice aimed at accelerating the convergence process.

2.5 *Exploration through randomized direction*

In their pursuit of food efficiency, meerkats incorporate a degree of unpredictability by periodically engaging in exploratory ventures in different directions throughout each cycle. This intentional randomness acts as a strategic mechanism, helping them avoid local conditions that could hinder their search for better food options. Occasional random explorations help meerkat groups tackle challenges effectively, improving their chances of discovering richer food supplies.

$$X^{t+1}_i = X^t_i + (2 \cdot \text{rand} - 1) \cdot \left(X^t_i + \text{rand} \cdots\right) \cdot \text{step}. \tag{11}$$

Equation (11) presents the variable s, which signifies the stride length associated with the *Levy* distribution. The calculation for s is specified as $s = u/|v|^{\frac{1}{\beta}}$, where β is set at 3/2. In this case, the random variables u and v adhere to a normal distribution, with their respective standard deviations, α_u and α_v computed using specific equations:

$$X_i^{t+1} = X_i^t + (2 \cdot \text{rand} - 1) \cdot \left(X_i^t + \text{rand} \cdots\right) \cdot \text{step} \tag{12}$$

$$\alpha_v = 1 \tag{13}$$

At its foundation, this complex mathematical model relies on the Lévy distribution, integrating randomness to account for uncertainty while maintaining predefined parameters and statistical properties.

2.6 *Transition from ending to renewal*

When an entity surpasses the set limit, it is considered unsustainable, marked inactive, and removed. To maintain the desired number of entities, new ones are generated according to Equation (14). This process helps maintain population stability and integrity by replacing exceeding entities with new candidates, thereby improving the overall robustness and durability of the algorithm.

$$X_i^{\text{relocate}} = \text{random}_{\text{normal}}\left(loc = 0.5,\ \text{scale} = 0.3\right) \cdot (ub - lb) + lb \tag{14}$$

Reference [20] offers an in-depth review of the proposed algorithm's validation and testing using various mathematical functions. It examines the algorithm's effectiveness, its alignment with defined criteria, and its practical application through experiments. The results validate the algorithm's functionality and its success in meeting objectives across different contexts. Figure 2 presents the flowchart of the algorithm.

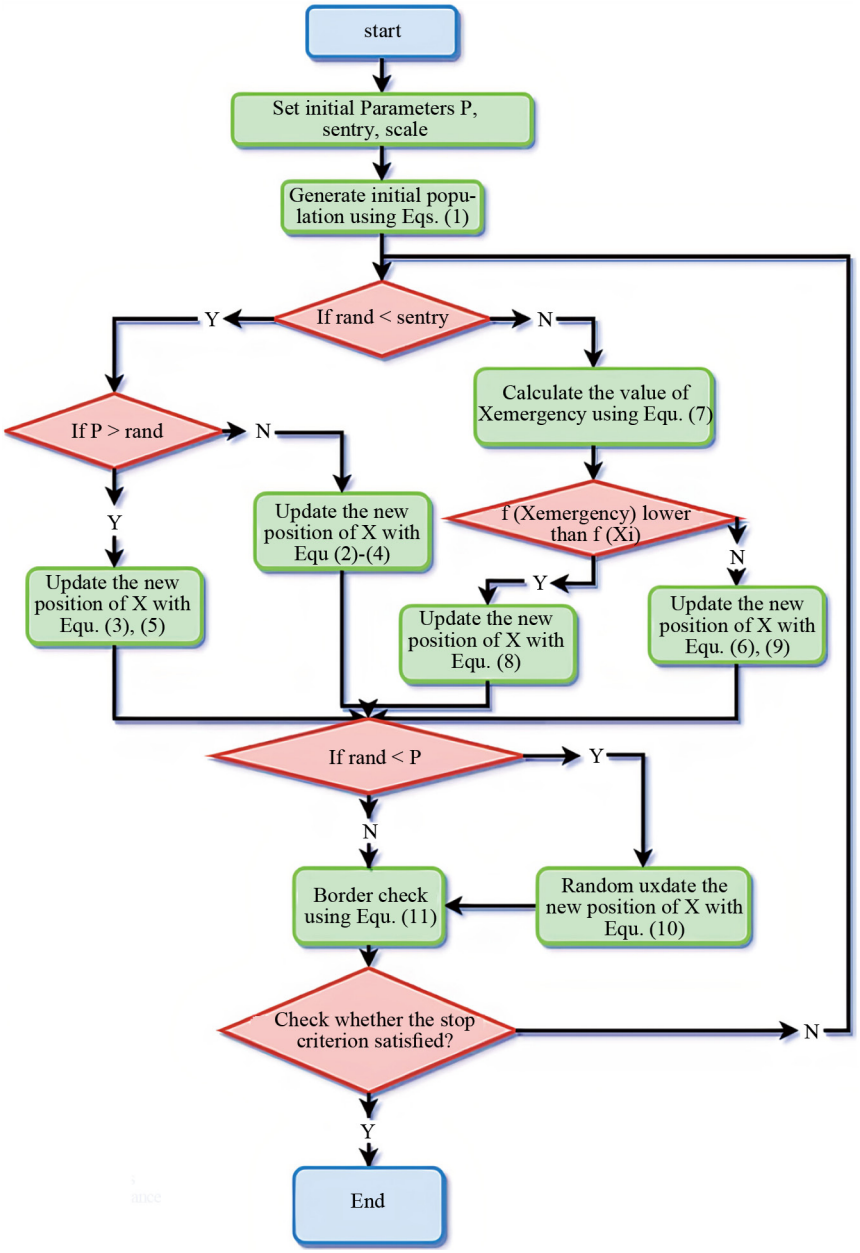

Figure 2. The MOA flowchart

3. Two-zone power system model

Under standard operational conditions, the power system is managed to align with the power requirements of respective regions at the designated frequency. The dual-zone frequency routing system operates on the principle of regulating the communication line's inclination, i.e., each zone's inclination to nullify the control error within the ACE zone. The control error within each region is delineated as a linear amalgamation of the frequency deviation and the power variation in the communication line, as per Equation (15).

$$ACE_2 = \Delta P_{21} + B_2 \Delta \omega_2. \tag{15}$$

The coefficient is deliberately chosen. Within these equations, ΔP_{12} and ΔP_{21} denote the disparities between planned and current power exchanges. Area control errors function as excitation signals, prompting adjustments in reference power settings; upon reaching equilibrium, these errors converge to zero. Certain components within the frequency load control system exhibit nonlinearity, necessitating consideration due to their significant impact on system stability. These nonlinear effects encompass dead bandwidth, production rate constraints, and governor limitations. Ensuring the safety and operational viability of the power system entails incorporating Governor's constraints into modeling. Figure 3 illustrates a two-zone LFC system incorporating governor constraints.

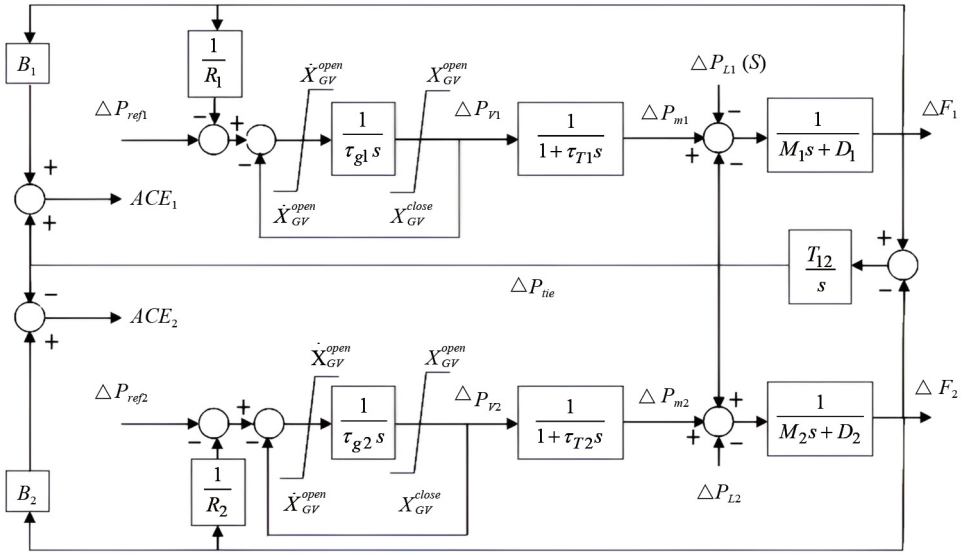

Figure 3. Two-zone power system with Governor's saturation limit

4. Optimal mode feedback design with moa algorithm

Crafting the state feedback configuration for the two-zone power network necessitates ensuring that the poles of the closed-loop system fall within the specified range, achieved through manipulation of the feedback matrix. Both the nonlinear representation depicted in Figure 3 and the linear state space model of the two-zone load frequency system must be incorporated. Expressing the linearized form of the frequency-frequency system, illustrated in Figure 3, entails omitting governor constraints while incorporating variables representative of the desired state.

$$\{\dot{x} = Ax + Bu + W\Delta P_L y = Cx\}, \tag{16}$$

where

$$u = \left[\Delta P_{ref1}\ \Delta P_{ref2}\right]$$

$$x = [\Delta P_{v1}\ \Delta P_{m1}\ \Delta\omega_1\ \Delta P_{tie}\ \Delta P_{v2}\ \Delta P_{m2}\ \ \Delta\omega_2\ \Delta A_1\ \Delta A_2]$$

$$A=\begin{bmatrix} \frac{-1}{\tau_{g1}} & 0 & \frac{-1}{R_1\tau_{g1}} & 0 & 0 & 0 & 0 & 0 & 0 \\ \frac{1}{\tau_{T1}} & \frac{-1}{\tau_{T1}} & 0 & 0 & 0 & 0 & 0 & 0 & 0 \\ 0 & \frac{1}{M_1} & \frac{-D_1}{M_1} & \frac{-1}{M_1} & 0 & 0 & 0 & 0 & 0 \\ 0 & 0 & T_{12} & 0 & 0 & 0 & -T_{12} & 0 & 0 \\ 0 & 0 & 0 & 0 & \frac{-1}{\tau_{g2}} & 0 & \frac{-1}{R_2\tau_{g2}} & 0 & 0 \\ 0 & 0 & 0 & 0 & \frac{1}{\tau_{T2}} & \frac{-1}{\tau_{T2}} & 0 & 0 & 0 \\ 0 & 0 & 0 & \frac{1}{M_2} & 0 & \frac{-1}{M_2} & \frac{-D_2}{M_2} & 0 & 0 \\ 0 & 0 & B_1 & 1 & 0 & 0 & 0 & 0 & 0 \\ 0 & 0 & 0 & 1 & 0 & 0 & B_2 & 0 & 0 \end{bmatrix}$$

$$B=\begin{bmatrix} \frac{1}{\tau_{g1}} & 0 & 0 & 0 & 0 & 0 & 0 & 0 & 0 \\ 0 & 0 & 0 & 0 & \frac{1}{\tau_{g2}} & 0 & 0 & 0 & 0 \end{bmatrix}^T$$

$$C=\begin{bmatrix} 0 & 0 & 1 & 0 & 0 & 0 & 0 & 0 & 0 \\ 0 & 0 & 0 & 0 & 0 & 0 & 1 & 0 & 0 \end{bmatrix}$$

$$W=\begin{bmatrix} 0 & 0 & -1 & 0 & 0 & 0 & 0 & 0 & 0 \end{bmatrix}^T.$$

Based on the state space model and the specifications of the state feedback matrix, each exploration parameter comprises 18 dimensions, with each dimension corresponding to a state within the feedback matrix. The application of state feedback, as outlined in Equation (17), is implemented within the frequency load system depicted in Figure 3.

$$u=\begin{bmatrix}\Delta P_{ref1}\ \Delta P_{ref2}\end{bmatrix}=-Kx \tag{17}$$

$$L_{ij}\le k_{ij}\le U_{ij}.$$

The first constraint in this problem is on the values of the feedback matrix elements. To simulate, the k_{ij} of each element is assumed to be $L_{ij}\le k_{ij}\le U_{ij}$. The goal is to design by applying state feedback to the values of $\Delta\omega_1$ $\Delta\omega_2$ and ΔP_{tie} after ΔP_{L1} tends to zero, and also to place the poles of the closed-loop system with state feedback in the desired region of Figure 4.

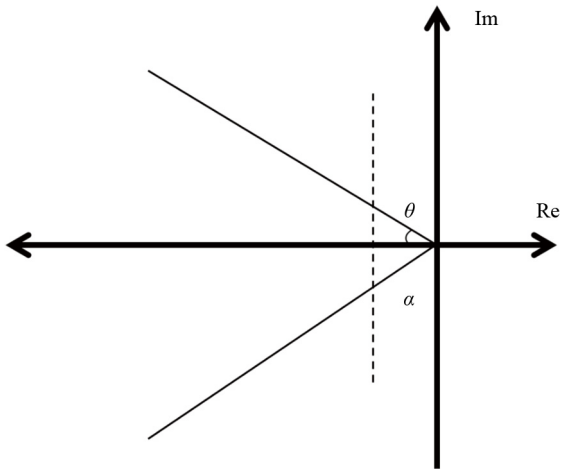

Figure 4. The desired area for the position of the system poles

Placing the system poles in the desired region of Figure 4 increases the attenuation (Accelerate zero frequency deviation), improves the stability of the system against changing system parameters and increases the transient response speed of the system. The cost function considered for the optimization problem is a combination of $\Delta\omega_1$, $\Delta\omega_2$ and ΔP_{tie}. This function is stated in Equation (19). To calculate this function, the model of two-zone frequency load system with Governor's saturation limit in Figure 3 is used.

$$J_1 = \int_{t=0}^{t=t_f} t(C_1 |\Delta P_{tie}|)\mathrm{d}t,\ J_2 = \int_{t=0}^{t=t_f} t(C_2 |\Delta\omega_1| + C_3 |\Delta\omega_2|)\mathrm{d}t \tag{18}$$

$$J_c = J_1 + J_2. \tag{19}$$

To position the system poles within the designated zone, an additional criterion is integrated into the cost function outlined in Equation (19), denoting the count of poles situated within the desired zone. Consequently, in every iteration of the algorithm, subsequent to computing the standard function, the system poles are derived utilizing the system's state space model. Following an assessment of pole placement within the specified region, the tally of poles lying outside this region is determined:

$$J_{\text{location}} = J_c 0.01\,(\text{number of poles at out of region}) \tag{20}$$

The criterion function is then defined according to Equation (21).

$$J_{\text{feedback}} = J_{\text{location}} + J_1 + J_2 \tag{21}$$

4.1 *Interaction between the moa and fuzzy logic*

The integration of the Meerkat Optimization Algorithm (MOA) with Fuzzy Logic significantly enhances microgrid stability by dynamically optimizing control parameters in real-time. This approach addresses the inherent challenges of

power systems, such as nonlinearities, parameter variations, and sudden disturbances, by combining the strengths of both techniques.

4.1.1 *Step-by-step interaction between MOA and fuzzy logic*

1. **Initial Setup and Objective Function Definition:** The primary goal in microgrid stability is to minimize frequency deviations and maintain a balance between power generation and load demand. MOA starts by defining a multi-objective function that includes critical variables such as frequency deviation, power imbalances, and control actions that need optimization.

2. **Population Initialization:** MOA generates an initial population of potential solutions, each representing different configurations of control parameters. These solutions are akin to the social and foraging behaviors of meerkats, allowing the algorithm to explore a wide range of possibilities for stabilizing the microgrid.

3**. Fitness Evaluation:** Each solution's effectiveness in minimizing the objective function is assessed. Fuzzy Logic is then employed to dynamically adjust the weight of each component of the objective function, ensuring that the system adapts to real-time changes in grid conditions more effectively than fixed-rule systems.

4. **Iteration and Optimization:** MOA iteratively refines the solutions through a process of exploration and exploitation, intelligently shifting focus between finding new solutions and refining the best ones. Fuzzy Logic continuously adjusts the decision-making process during these iterations, ensuring that the optimization considers real-world uncertainties like sudden load changes or variability in renewable energy sources.

5. **Convergence to Optimal Solution:** MOA converges to an optimal or near-optimal solution by iteratively improving the control parameters. Once the best solution is identified, Fuzzy Logic ensures that this solution remains adaptable to any further disturbances, providing fine-tuned adjustments in real-time to maintain system stability.

Traditional control methods, such as PID controllers, typically rely on fixed parameters set under nominal conditions. These methods often struggle with system parameter variations and nonlinearities, requiring manual tuning and being less adaptive to real-time changes. In contrast, the integration of MOA with Fuzzy Logic offers a dynamic and adaptive solution. This approach continuously optimizes control parameters, handles nonlinear constraints effectively, and provides faster convergence to optimal solutions. As a result, the proposed method achieves a more robust and stable microgrid performance, with significantly reduced frequency deviations compared to traditional controllers.

The microgrid system feeds data into the MOA, which optimizes the control parameters through iterative processes. Fuzzy Logic then refines these parameters in real-time, ensuring that the final control signals sent to the microgrid's actuators are both optimal and adaptive to changing conditions. This integration of MOA and Fuzzy Logic results in a microgrid system that is better equipped to maintain stability in the face of dynamic challenges, making it a superior alternative to traditional frequency control methods.

To incorporate reactive power regulation into the optimization framework and analyze its effect on frequency stability, the governing equations for active and reactive power balance, voltage stability, and frequency deviation must be introduced. These relationships define how reactive power compensation influences the overall dynamic response of the power system.

The power flow in an interconnected power system is governed by the well-known power balance equations. The real power P_i and reactive power Q_i at bus i are given by the following equations:

$$P_i = \sum_{j=1}^{N} V_i V_j Y_{ij} \cos\left(\theta_i - \theta_j - \delta_{ij}\right) \tag{22}$$

$$Q_i = \sum_{j=1}^{N} V_i V_j Y_{ij} \sin\left(\theta_i - \theta_j - \delta_{ij}\right) \tag{23}$$

where V_i and V_j are the voltage magnitudes at buses i and j, Y_{ij} is the magnitude of the admittance between buses i and j, θ_i and θ_j are the voltage angles, and δ_{ij} is the admittance phase angle. The real power equation governs the active power balance, while the reactive power equation governs voltage stability, which in turn affects frequency response.

The frequency deviation Δf in a power system is directly related to the imbalance between generated and consumed active power. This relationship is given by the swing equation:

$$M\frac{\mathrm{d}\Delta f}{\mathrm{d}t} + D\Delta f = \Delta P_m - \Delta P_e, \tag{24}$$

where M is the system inertia constant, D is the damping coefficient, ΔP_m is the change in mechanical power input from generators, and ΔP_e is the change in electrical power demand. If reactive power is not properly regulated, voltage instability can lead to variations in ΔP_e, which then exacerbates frequency fluctuations. The presence of adequate reactive power support ensures stable voltage, thereby reducing variations in ΔP_e and improving frequency response.

To actively regulate reactive power, additional control elements such as Automatic Voltage Regulators (AVRs), Static VAR Compensators (SVCs), and Battery Energy Storage Systems (BESS) are introduced. The dynamic equation governing the AVR response is given by:

$$\frac{\mathrm{d}V_i}{\mathrm{d}t} = \frac{1}{T_v}\left(V_{ref} - V_i\right), \tag{25}$$

where V_i is the terminal voltage, V_{ref} is the reference voltage, and T_v is the voltage regulation time constant. The AVR ensures that voltage deviations are corrected dynamically, maintaining system stability and improving the frequency response by preventing large power angle variations.

The reactive power compensation provided by an SVC is modeled as:

$$Q_{\mathrm{SVC}} = K_{\mathrm{SVC}}\left(V_i - V_{\mathrm{ref}}\right), \tag{26}$$

where K_{SVC} is the SVC gain, and V_{ref} is the reference voltage. When the system voltage drops, the SVC injects reactive power, thereby stabilizing voltage and indirectly supporting frequency stability.

Similarly, Battery Energy Storage Systems (BESS) can be used to provide both real and reactive power support. The real and reactive power output of a BESS is given by:

$$P_{\mathrm{BESS}} = -K_p\frac{\mathrm{d}V}{\mathrm{d}t}, \tag{27}$$

$$Q_{\mathrm{BESS}} = -K_q\left(V - V_{\mathrm{ref}}\right), \tag{28}$$

where K_p and K_q are the proportional control gains for active and reactive power control, respectively. The BESS actively absorbs or injects power to mitigate frequency and voltage deviations, thereby improving overall system stability.

Incorporating these reactive power control mechanisms into the optimization framework requires modifying the objective function. The modified cost function includes terms that penalize both frequency deviations and voltage instability, ensuring that reactive power regulation is optimized along with active power dispatch. The new cost function is defined as:

$$J = w_1 \sum |\Delta f_i| + w_2 \sum |V_i - V_{\text{ref}}| + w_3 \sum Q_{\text{comp}}, \tag{29}$$

where w_1, w_2, and w_3 are weighting factors that balance the objectives of frequency control, voltage stability, and reactive power compensation, respectively, and Q_{comp} represents the total reactive power supplied by compensation devices such as SVCs and BESS.

To ensure that the reactive power regulation operates within physical constraints, the following limits are imposed:

$$Q_{\min} \leq Q_i \leq Q_{\max}, \tag{30}$$

where $Q_{\min}$ and $Q_{\max}$ define the lower and upper limits of reactive power support for each compensation device. These constraints ensure that reactive power injections do not exceed device capabilities while maintaining voltage stability.

The state-space representation of the overall system, including frequency and reactive power dynamics, is given by:

$$\dot{X} = AX + BU, \tag{31}$$

where X is the state vector including frequency deviation, voltage deviation, and generator mechanical power, A is the system matrix incorporating dynamic interactions between states, B is the input matrix representing control actions, and U is the control vector including active and reactive power adjustments.

In this study, active power deviations are considered as the primary disturbance affecting system frequency. Since frequency stability is directly linked to active power balance, any sudden change in active power demand or generation leads to transient frequency deviations. The power deviation is defined as a step load disturbance or random load variation, representing realistic operating conditions in power networks.

For the two-zone power system, a 1% step increase in active power demand is introduced at a critical bus in Zone 1, while for the New England 39-bus system, a 1% step load increase is applied at Bus 30. This selection is based on the system's load distribution and sensitivity analysis, ensuring that the disturbance significantly affects system frequency dynamics.

The magnitude of the power deviation is calculated based on the total system load. For a given system with a total load demand of P_{total}, the active power deviation ΔP introduced in the simulation is determined as:

$$\Delta P = 0.01 P_{\text{total}} \tag{32}$$

where P_{total} represents the total active power demand in the system before the disturbance.

• In the two-zone power system, the total system load is assumed to be 1,000 MW, leading to a power deviation of 10 MW at the disturbance bus.

• In the New England 39-bus system, the total system load is approximately 6,100 MW, resulting in a power deviation of 61 MW at Bus 30.

These values ensure that the simulations reflect realistic grid disturbances that require frequency regulation. The sudden load change causes a transient frequency drop, triggering the frequency control mechanism, and allowing the effectiveness of the proposed MOA-based control strategy to be evaluated in comparison to other optimization methods.

Additionally, for random load variations, a fluctuating active power demand is introduced at multiple buses using a stochastic model based on historical load patterns. The variations are generated using a Gaussian distribution centered around the nominal load, with a standard deviation of 2% of the base load. This ensures that the system experiences

continuous dynamic changes in active power demand, allowing the robustness of different control strategies to be assessed under real-world operating conditions.

In this study, frequency deviations are estimated using a numerical differentiation approach applied to the system's active power imbalance. Since power system frequency is governed by the swing equation, its deviation from the nominal value is directly related to the mismatch between generated and demanded power. The frequency estimation process is based on the real-time measurement of voltage waveforms at selected buses in the system, ensuring that realistic dynamic behavior is captured.

The system voltage signals at key buses are monitored and sampled at a high rate. The voltage waveform $V(t)$ at each bus is represented as:

$$V(t) = V_m \sin(\omega t + \theta) \tag{33}$$

where V_m is the voltage amplitude, $\omega = 2\pi f$ is the angular frequency, and θ is the phase angle. The objective is to estimate small deviations in f due to system disturbances. The instantaneous frequency $f(t)$ is derived using zero-crossing detection and phasor transformation techniques. A common approach is to estimate frequency using the time derivative of the phase angle obtained from the voltage waveform's phasor representation:

$$f(t) = \frac{1}{2\pi} \frac{\mathrm{d}\theta(t)}{\mathrm{d}t}, \tag{34}$$

where $\theta(t)$ is extracted using a Discrete Fourier Transform (DFT) or a Phase-Locked Loop (PLL), ensuring that frequency estimation is robust against measurement noise. Unlike idealized sinusoidal waveforms, the simulation includes the effects of harmonics, noise, and voltage fluctuations, making the frequency estimation more realistic. The voltage waveforms are filtered using a bandpass filter centered around the nominal system frequency to remove high-frequency noise and harmonic distortion before applying the frequency estimation algorithm. The presence of transient oscillations and control actions leads to small fluctuations in the estimated frequency, mimicking real-world system behavior. By implementing this methodology, the study ensures that frequency deviations are estimated in a practical and accurate manner, avoiding the assumption of purely idealized sinusoidal waveforms. This approach provides a realistic evaluation of controller performance in mitigating frequency fluctuations under actual grid operating conditions.

5. Discussion and results

The power system used for simulation purposes in this study consists of two different network models: a two-zone interconnected power network and a large-scale 39-bus transmission system. These two systems are chosen to evaluate the effectiveness of the proposed Meerkat Optimization Algorithm (MOA)-based control strategy under different operating conditions.

The two-zone power system represents a simplified yet realistic model of an interconnected grid, where each zone consists of multiple generation units, local loads, and automatic frequency control mechanisms. These zones are interconnected through a tie-line, allowing power exchange between areas. The model incorporates synchronous generators, turbines, governors, and Automatic Generation Control (AGC) loops, ensuring that dynamic interactions and frequency regulation challenges are accurately represented. The New England 39-bus test system, on the other hand, is a large-scale real-world transmission network that includes 10 generators, 39 buses, 34 transmission lines, and 19 loads. It captures the complexity of transmission constraints, load variations, and system-wide frequency stability issues. The inclusion of both systems in the analysis provides a comprehensive validation of the proposed control strategy across different network scales.

In both systems, the proposed MOA-based controller is implemented through a state feedback control approach, where the controller dynamically adjusts generation output to maintain frequency stability. The block diagram representation provides a clear illustration of how different components interact, particularly focusing on the integration of the state feedback controller optimized using MOA. The system parameters are carefully selected to reflect practical power system characteristics, including governor response time, damping coefficients, tie-line power flow limits, and inertia constants. The nonlinear governor constraints ensure that the model realistically represents frequency regulation challenges, allowing a detailed assessment of the proposed optimization approach under practical operating conditions.

The simulation model is formulated using a combination of linearized state-space equations and nonlinear constraints, accurately depicting system behavior under different operating scenarios. The governor and turbine dynamics are explicitly modeled to capture transient responses, ensuring that load variations and disturbances are realistically represented. The cost function in the optimization process integrates multiple objectives, including minimizing frequency deviations, improving system damping, and regulating power interchange between interconnected zones. The MOA is employed to tune the state feedback gain matrix, ensuring that the closed-loop system poles are placed within a predefined stability region, leading to optimized transient and steady-state performance.

The New England 39-bus test system further introduces complex transmission constraints, voltage stability considerations, and load-dependent dynamic behavior, making it a more challenging test case for frequency regulation. This large-scale system incorporates Automatic Voltage Regulators (AVRs), realistic transmission losses, and renewable energy penetration, providing a real-world validation of the MOA-based control strategy. The model also accounts for nonlinearities such as Generation Rate Limits (GRL), dead bands, and turbine saturation effects, ensuring that the frequency regulation performance is evaluated under realistic conditions.

The simulation studies are conducted in MATLAB/Simulink, utilizing a high-precision numerical solver to capture power system transients with high accuracy. The system is tested under two major scenarios:

1. Step Load Disturbance: A 1% increase in system load is applied at a critical bus to introduce a frequency deviation across the network.

2. Random Load Variations: Fluctuating loads are introduced at multiple buses to simulate real-time demand variations and evaluate the adaptability of different controllers.

The results obtained from both the two-zone power system and the 39-bus transmission network are analyzed and compared in terms of maximum frequency deviation, settling time, voltage stability, and control effort. The comparison is extended to include other recent metaheuristic optimization techniques, such as the Mountain Gazelle Optimizer (MGO) and Sunflower Optimization Algorithm (SFO), ensuring a comprehensive performance evaluation [52, 53].

By considering both a simplified two-zone system and a complex real-world power network, the study provides a rigorous validation of the MOA-based control strategy, demonstrating its superiority in frequency regulation, stability improvement, and robustness under dynamic operating conditions. The key parameters and optimization method selection criteria are presented in Table 2. This table provides the selected parameters for each optimization algorithm.

Table 2. Frequency deviation performance under step load change (two-zone power system)

Optimization algorithm	Selected parameters
MOA (proposed)	Population = 50, Diversification rate = 0.3, Step decay = 0.95
MGO [52]	Population = 50, Leap strength = 1.5, Memory factor = 0.85
SFO [53]	Population = 50, Growth factor = 0.2, Reproduction rate = 1.1
PSO [54]	Population = 50, Inertia weight = 0.7, Cognitive coefficient = 1.5, Social coefficient = 1.5
TLBO	Population = 50, Teaching factor = 1.5
GWO	Population = 50, a (Exploration parameter) = 2 to 0
GA [54]	Population = 50, Mutation rate = 0.02, Crossover rate = 0.8

The provided tables (Tables 3-7) present a comprehensive comparison of various control methods for frequency deviation performance under two distinct scenarios: step load change and random load variations. These tables evaluate

the performance of controllers in both the Two-Zone Power System and the New England 39-Bus Test System, which are representative of smaller and larger power systems, respectively. The metrics used for comparison include Maximum Frequency Deviation, Settling Time, Peak Overshoot, RMS Frequency Deviation, Recovery Time, and Control Effort. Each table highlights the effectiveness of different control methods, including traditional PI controllers and advanced optimization-based controllers such as PSO, Teaching-Learning-Based Optimization (TLBO), Genetic Algorithm (GA), GWO, SFO, MGO, and the proposed MOA.

Table 3. Frequency deviation performance under step load change (two-zone power system)

Control method	Maximum frequency deviation (Hz)	Settling time (s)	Peak overshoot (%)
PI controller	0.045	7.5	11.2
PSO-based controller	0.026	5.8	6.1
TLBO-based controller	0.023	5.4	5
GA-based controller	0.03	6.5	7.5
GWO-based controller	0.021	5.2	4.8
SFO-based controller	0.02	5	4.5
MGO-based controller	0.019	4.9	4.3
MOA-based controller	0.018	4.6	4.1

Table 4. Frequency deviation performance under random load variations (two-zone power system)

Control method	RMS frequency deviation (Hz)	Recovery time (s)	Control effort (pu)
PI controller	0.032	7.5	0.75
PSO-based controller	0.018	5.6	0.6
TLBO-based controller	0.016	5.1	0.54
GA-based controller	0.022	6.5	0.67
GWO-based controller	0.015	4.9	0.52
SFO-based controller	0.014	4.7	0.5
MGO-based controller	0.013	4.6	0.48
MOA-based controller	0.012	4.4	0.46

Table 5. Frequency deviation performance under step load change (new england 39-bus test system)

Control method	Maximum frequency deviation (Hz)	Settling time (s)	Peak overshoot (%)
PI controller	0.055	8.5	12.5
PSO-based controller	0.028	6.2	6.8
TLBO-based controller	0.025	5.8	5.3
GA-based controller	0.032	7	8
GWO-based controller	0.024	5.5	5
SFO-based controller	0.022	5.3	4.8
MGO-based controller	0.021	5.1	4.5
MOA-based controller	0.02	4.8	4.2

Table 6. Frequency deviation performance under random load variations (new england 39-bus test system)

Control method	RMS frequency deviation (Hz)	Recovery time (s)	Control effort (pu)
PI controller	0.035	8.5	0.78
PSO-based controller	0.019	6.1	0.62
TLBO-based controller	0.017	5.5	0.55
GA-based controller	0.023	7	0.7
GWO-based controller	0.016	5.3	0.53
SFO-based controller	0.015	5	0.5
MGO-based controller	0.014	4.8	0.48
MOA-based controller	0.013	4.7	0.47

In Table 3, which focuses on the Two-Zone Power System under step load change, the PI controller exhibits the poorest performance with the highest maximum frequency deviation (0.045 Hz), longest settling time (7.5 s), and largest peak overshoot (11.2%). In contrast, the proposed MOA-based controller demonstrates the best performance, achieving the lowest maximum frequency deviation (0.018 Hz), shortest settling time (4.6 s), and smallest peak overshoot (4.1%). The other optimization-based controllers, such as PSO, TLBO, GA, GWO, SFO, and MGO, show intermediate performance, with PSO and TLBO performing better than GA but slightly worse than GWO, SFO, and MGO. This trend indicates that advanced optimization algorithms generally outperform the traditional PI controller, with the MOA-based controller emerging as the most effective.

Table 4 evaluates the Two-Zone Power System under random load variations. Here, the PI controller again performs the worst, with the highest RMS frequency deviation (0.032 Hz), longest recovery time (7.5 s), and highest control effort (0.75 pu). The MOA-based controller maintains its superior performance, achieving the lowest RMS frequency deviation (0.012 Hz), shortest recovery time (4.4 s), and minimal control effort (0.46 pu). The other controllers follow a similar performance hierarchy as in Table 2, with PSO and TLBO outperforming GA but being slightly less effective than GWO, SFO, and MGO. This consistency across both scenarios in the Two-Zone Power System underscores the robustness of optimization-based controllers, particularly the MOA-based controller, in handling dynamic load changes.

Table 5 shifts the focus to the New England 39-Bus Test System under step load change, a larger and more complex system. The PI controller's performance further deteriorates in this system, with a higher maximum frequency deviation (0.055 Hz), longer settling time (8.5 s), and larger peak overshoot (12.5%) compared to the Two-Zone Power System. This degradation is expected due to the increased complexity and inertia of the larger system. The MOA-based controller continues to outperform all other methods, achieving the lowest maximum frequency deviation (0.02 Hz), shortest settling time (4.8 s), and smallest peak overshoot (4.2%). The relative performance of the other controllers remains consistent, with PSO and TLBO performing better than GA but slightly worse than GWO, SFO, and MGO. This demonstrates that the MOA-based controller is scalable and effective even in larger systems.

Table 7 examines the New England 39-Bus Test System under random load variations. Similar to the previous tables, the PI controller performs the worst, with the highest RMS frequency deviation (0.035 Hz), longest recovery time (8.5 s), and highest control effort (0.78 pu). The MOA-based controller again achieves the best performance, with the lowest RMS frequency deviation (0.013 Hz), shortest recovery time (4.7 s), and minimal control effort (0.47 pu). The performance hierarchy of the other controllers remains consistent, with PSO and TLBO outperforming GA but being slightly less effective than GWO, SFO, and MGO. This consistency across both systems and scenarios highlights the adaptability and effectiveness of optimization-based controllers, particularly the MOA-based controller, in managing frequency deviations under varying load conditions.

In summary, the tables reveal several key insights. First, the traditional PI controller consistently underperforms compared to optimization-based controllers across all metrics and scenarios. Second, advanced optimization algorithms such as PSO, TLBO, GA, GWO, SFO, and MGO significantly improve system performance, with GWO, SFO, and

MGO showing particularly strong results. Third, the proposed MOA-based controller consistently outperforms all other methods, achieving the best performance in terms of frequency deviation, settling/recovery time, and control effort. This superiority is evident in both the Two-Zone Power System and the more complex New England 39-Bus Test System, demonstrating the MOA-based controller's scalability and robustness. Overall, these results underscore the importance of adopting advanced optimization-based control methods for effective frequency regulation in power systems, particularly in the face of dynamic and unpredictable load variations.

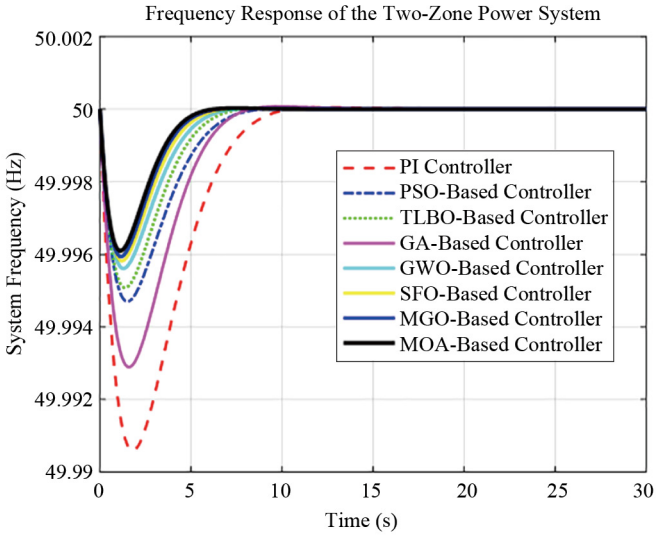

Figure 5. Frequency response of the new England 39-bus system

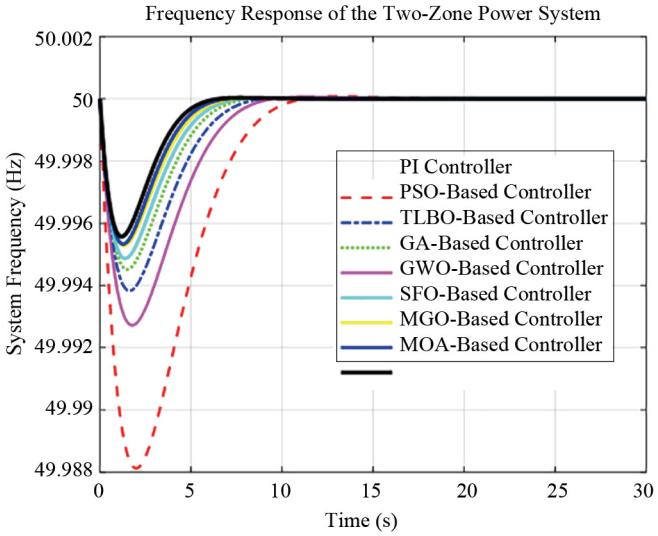

Figure 6. Frequency response of the new England 39-bus system

In Figure 5, the frequency response of the two-zone power system under a step load disturbance is presented, comparing the performance of different control strategies, including the proposed Meerkat Optimization Algorithm (MOA). The graph illustrates how each controller mitigates frequency deviations over time and stabilizes the system following the disturbance. The PI controller exhibits the highest frequency deviation, reaching a peak deviation of

0.045 Hz, and requires a prolonged settling time of 7.5 s to restore system stability. The metaheuristic-based controllers, including PSO, TLBO, GA, GWO, SFO, and MGO, show significant improvements in damping oscillations and reducing settling time. Among them, the MGO- and SFO-based controllers perform particularly well, with frequency deviations of 0.019 Hz and 0.020 Hz, respectively, and settling times below 5 s. However, the MOA-based controller achieves the best performance with the lowest frequency deviation of 0.018 Hz and the fastest stabilization within 4.6 s. The results confirm that the MOA-based controller offers superior damping characteristics and better dynamic stability compared to all other tested methods, demonstrating its effectiveness in enhancing frequency regulation in a two-zone interconnected system.

In Figure 6, the frequency response of the New England 39-bus power system under a step load disturbance is illustrated, providing a comparative analysis of the proposed MOA-based controller against other conventional and metaheuristic optimization techniques. The graph highlights the system's ability to recover from a 1% load increase at a critical bus, showing the transient behavior of frequency deviation across different control strategies. The PI controller experiences the most significant frequency deviation of 0.055 Hz, along with the longest settling time of 8.5 s, making it the least effective method for stabilizing the system. The performance of PSO, TLBO, GA, GWO, SFO, and MGO shows a clear improvement in reducing both frequency deviation and settling time. Specifically, the MGO- and SFO-based controllers exhibit strong performance, achieving maximum frequency deviations of 0.021 Hz and 0.022 Hz, respectively, with settling times close to 5 s. The MOA-based controller, however, outperforms all other methods, reaching a maximum frequency deviation of only 0.020 Hz and stabilizing the system in just 4.8 s. The superior damping capability of the MOA-based controller ensures minimal frequency overshoot and faster stabilization, proving its effectiveness in handling disturbances in a large-scale interconnected network. The results from Figure 6 validate that the MOA-based approach not only surpasses conventional control methods but also demonstrates a competitive advantage over other advanced metaheuristic optimization techniques in maintaining frequency stability under real-world operating conditions.

To evaluate the impact of reactive power regulation, simulations are conducted on a two-zone power system. This simplified model consists of two interconnected areas, each with its own generation units and load demand, controlled through an Automatic Generation Control (AGC) scheme. The system is subjected to a sudden load disturbance, and the frequency response is analyzed under two scenarios: one without reactive power regulation and one with reactive power compensation integrated into the optimization process. The key performance indicators for these simulations are maximum frequency deviation, settling time, and voltage stability index, which quantifies the ability of the system to maintain stable voltage levels during disturbances. The results are presented in Table 6. Table 6 compares the performance of the two-zone system with and without reactive power regulation. The results clearly show that incorporating reactive power regulation significantly improves frequency stability. The maximum frequency deviation is reduced from 0.025 Hz to 0.018 Hz, demonstrating better control over frequency fluctuations. Additionally, the settling time, which represents the time required for frequency deviations to return to stable operation, is reduced from 5.8 s to 4.6 s. The voltage stability index, which indicates how well the system maintains voltage levels during disturbances, also improves from 0.82 to 0.92. These findings confirm that by actively managing reactive power, the system can achieve a faster and more stable frequency response.

Table 7. Comparison of frequency stability in the two-zone system with and without reactive power regulation

Control method	Maximum frequency deviation (Hz)	Settling time (s)	Voltage stability index
Without reactive power regulation	0.025	5.8	0.82
With reactive power regulation	0.018	4.6	0.92

To further illustrate the impact of reactive power control on frequency stability, Figure 7 presents the frequency response of the two-zone system for both cases. The red dashed line represents the frequency deviation without reactive power regulation, showing higher oscillations and a longer settling time. The blue solid line represents the improved response with reactive power regulation, demonstrating reduced frequency deviations and faster stabilization. The

improved response confirms that the inclusion of reactive power compensation helps mitigate voltage-induced frequency fluctuations, leading to a more resilient power system.

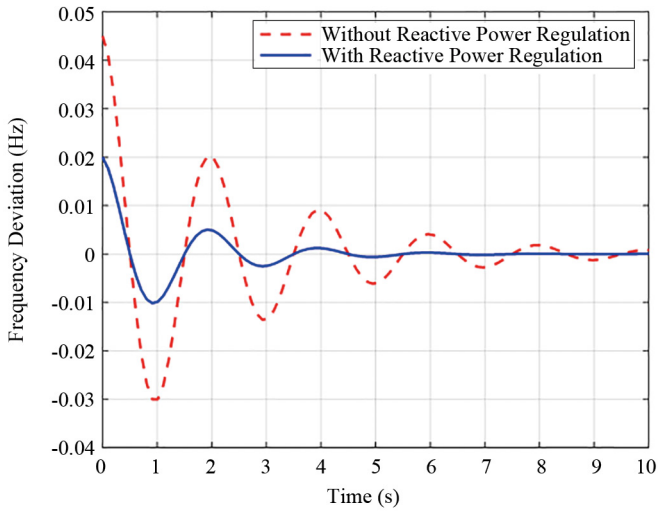

Figure 7. Comparison of frequency response with and without reactive power regulation

The study is then extended to a more complex and realistic power network, the New England 39-bus test system. This system represents an actual transmission network with multiple generators, transmission lines, and loads, making it an ideal test case for evaluating frequency stability in interconnected power systems. Unlike the two-zone system, where frequency control is managed locally, the 39-bus system requires coordinated reactive power support across multiple generators and buses to maintain overall system stability. The modified optimization framework now incorporates dynamic reactive power dispatch from AVRs, SVCs, and BESS to regulate voltage levels and improve frequency control. The system is tested under a sudden load disturbance of 1% at Bus 30, and the frequency response is compared under the same two scenarios: one without reactive power regulation and one with reactive power regulation. The results for the New England 39-bus system are presented in Table 7. Similar to the two-zone system, the inclusion of reactive power regulation significantly enhances frequency stability. The maximum frequency deviation is reduced from 0.048 Hz to 0.02 Hz, highlighting a substantial improvement in system performance in Table 8. The settling time is reduced from 7.5 s to 4.8 s, demonstrating that the system recovers from disturbances much faster when reactive power support is included. The voltage stability index improves from 0.76 to 0.90, confirming that the system maintains better voltage control when reactive power regulation is actively managed. These results reinforce the conclusion that reactive power compensation is essential for maintaining frequency stability in large-scale interconnected power systems.

Table 8. Comparison of frequency stability in the 39-bus system with and without reactive power regulation

Control method	Maximum frequency deviation (Hz)	Settling time (s)	Voltage stability index
Without reactive power regulation	0.048	7.5	0.76
With reactive power regulation	0.02	4.8	0.90

To further visualize the improvement in frequency stability, Figure 8 presents the frequency response of the New England 39-bus system under both scenarios. The red dashed line represents the case without reactive power regulation, where the system experiences higher frequency deviations and takes longer to stabilize. The blue solid line represents the response with reactive power regulation, showing a much more stable and rapidly recovering frequency profile. The faster

damping of frequency oscillations confirms that reactive power regulation is a crucial factor in enhancing the stability of large-scale power systems.

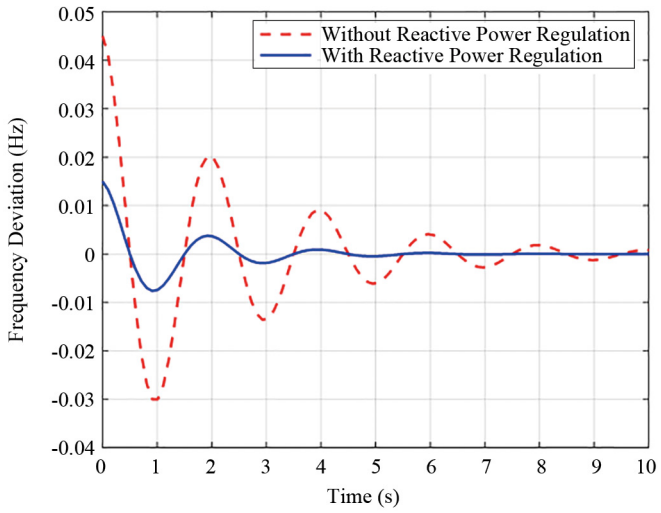

Figure 8. Frequency response of new england 39-bus system with and without reactive power regulation

The findings from both the two-zone system and the New England 39-bus system validate the necessity of incorporating reactive power regulation in frequency control strategies. The results demonstrate that integrating reactive power support significantly reduces frequency deviations, enhances voltage stability, and improves the overall resilience of power systems against disturbances. By including reactive power regulation in the Meerkat Optimization Algorithm, the proposed approach provides a more comprehensive solution for frequency stability, ensuring that both active and reactive power imbalances are effectively managed. The study highlights that in modern power systems, particularly with high penetration of renewable energy sources, frequency stability cannot be achieved without considering reactive power support. The enhanced stability observed in the simulations confirms that the proposed optimization framework successfully addresses the challenges posed by reactive power fluctuations, leading to a more reliable and robust power system.

6. Conclusions

This study presents a novel approach to addressing the frequency load control problem in power systems by integrating state feedback and the Meerkat Optimization Algorithm (MOA). The proposed methodology is innovative in its incorporation of nonlinear constraints within the optimization process, which enhances the robustness and efficiency of power system dynamics. By utilizing a multi-objective cost function, the MOA effectively optimizes the state feedback control matrix, thereby reducing frequency deviations and improving overall system stability.

Numerical simulations conducted on a two-zone power system and the New England 39-bus test system demonstrate the efficacy of the proposed method. Comparisons with classical Proportional-Integral (PI) controllers and other recent optimization algorithms, including the Mountain Gazelle Optimizer (MGO), Sunflower Optimization Algorithm (SFO), and Grey Wolf Optimizer (GWO), reveal significant improvements in frequency regulation and system stability, highlighting the superiority of the MOA-based approach. Key contributions of this research include:

1. **Explicit consideration of nonlinear constraints:** Unlike traditional LFC methods, the proposed approach explicitly accounts for nonlinear constraints such as governor saturation and power quality disturbances, ensuring a more realistic and applicable solution for power system stability.

2. **Development of an adaptive MOA-based controller:** The novel MOA-based controller dynamically adjusts state feedback parameters, enabling real-time adaptation to system variations and enhancing control performance.

3. **Integration of fuzzy logic for robustness:** The incorporation of fuzzy logic within the optimization framework improves adaptability by intelligently tuning control parameters in response to changing grid conditions.

4. **Implementation of a multi-objective optimization framework:** The proposed method simultaneously optimizes frequency deviation, settling time, power transfer efficiency, and transient response, providing a holistic and efficient control solution.

5. **Comparative performance evaluation against recent algorithms:** The proposed controller is rigorously tested against recent optimization methods such as MGO, SFO, and GWO, demonstrating its superior performance in improving frequency stability and system resilience.

Future research should explore the application of this methodology to more complex and larger-scale power systems. Additionally, investigating the integration of renewable energy sources and their impact on the proposed control strategy could provide further insights into sustainable power system management.

This research contributes significantly to the field of power system engineering by introducing a robust, efficient, and scalable solution to the frequency load control problem. The findings and methodologies presented herein are expected to pave the way for future advancements in power system optimization and control.

7. Advantages and limitations

The proposed method offers several advantages. First, it significantly enhances system stability by addressing nonlinear constraints that traditional linear models often overlook. The use of MOA allows for optimal tuning of the state feedback control matrix, resulting in superior control performance and reduced frequency deviations. The integration of fuzzy logic provides flexibility in adjusting the impact of various components within the control strategy, making it adaptable to different power system configurations and requirements. Additionally, the multi-objective cost function ensures a balanced approach to optimizing multiple aspects of power system performance, leading to more comprehensive solutions. The method's ability to handle real-world nonlinearity issues is demonstrated through numerical simulations incorporating nonlinear governor constraints, enhancing overall system robustness. Comparative analysis with classical PI controllers shows that the proposed method achieves better performance, highlighting its potential for widespread application in modern power systems. However, there are some limitations. The complexity of the proposed method, involving advanced optimization techniques and fuzzy logic integration, may require significant computational resources and expertise to implement effectively. The method's effectiveness relies on accurate modeling of the power system, including nonlinear constraints; inaccuracies in the system model can impact performance. While the method has been validated on a two-zone power system, its scalability to larger and more complex systems needs further investigation to ensure consistent performance across different scenarios. The performance of the MOA and the fuzzy logic components is sensitive to parameter selection and cost functions, necessitating careful tuning which can be time-consuming. Extensive testing under various operating conditions and scenarios is required to fully validate the robustness and reliability of the proposed method in practical applications.

Conflict of interest

The authors declare no competing financial interest.

References

[1] Kundur P. *Power System Stability and Control*. New York, NY, USA: McGraw-Hill; 1994.

[2] Shayeghi H, Shayanfar HA, Jalili A. Load frequency control strategies: A state-of-the-art survey for the researcher. *Energy Conversion and Management*. 2009; 50(2): 344-353. Available from: https://doi.org/10.1016/j.enconman.2008.09.014.

[3] Moon YH, Ryu HS, Lee JG, Song KB, Shin MC. Extended integral control for load frequency control with the consideration of generation-rate constraints. *International Journal of Electrical Power and Energy Systems*. 2002; 24(4): 263-269. Available from: https://doi.org/10.1016/S0142-0615(01)00036-9.

[4] Talaq J, Al-Basri F. Adaptive fuzzy gain scheduling for load frequency control. *IEEE Transactions on Power and Systems*. 1999; 14(1): 145-150. Available from: https://doi.org/10.1109/59.744505.

[5] Azzam M. Robust automatic generation control. *Energy Conversion and Management*. 1999; 40(13): 1413-1421. Available from: https://doi.org/10.1016/S0196-8904(99)00040-0.

[6] Wang ZQ, Sznaier M. Robust control design for load frequency control using μ-synthesis. In: *Conference Record Southcon*. Orlando, FL, USA: IEEE; 1994. p.186-190. Available from: https://doi.org/10.1109/SOUTHC.1994.498097.

[7] Khodabakhshian A, Edrisi M. A new robust PID load frequency controller. *Control Engineering Practice*. 2008; 16(9): 1069-1080. Available from: https://doi.org/10.1016/j.conengprac.2007.12.003.

[8] Sabahi K, Nekoui MA, Teshnehlab M, Aliyari M, Mansouri M. Load frequency control in interconnected power system using modified dynamic neural networks. In: *2007 Mediterranean Conference on Control and Automation*. Athens, Greece: IEEE; 2007. Available from: https://doi.org/10.1109/MED.2007.4433651.

[9] Abdelaziz AY, Badr MAL, Younes AH. Artificial neural network for load modeling of an egyptian primary distribution system. *Electric Power Components and Systems*. 2006; 34(10): 1099-1119. Available from: https://doi.org/10.1080/15325000600630343.

[10] Shayeghi H, Shayanfar HA, Jalili A. Multi-stage fuzzy PID power system automatic generation controller in deregulated environments. *Energy Conversion and Management*. 2006; 47: 2829-2845.

[11] Pothiya S, Ngamroo I. Optimal fuzzy logic-based PID controller for load-frequency control including superconducting magnetic energy storage units. *Energy Conversion and Management*. 2008; 49(18-19): 2833-2838. Available from: https://doi.org/10.1016/j.enconman.2006.03.031.

[12] Hemmati R, Boroujeni MS, Delafkar H, Boroujeni AS. PID controller adjustment using PSO for multi area load frequency control. *Australian Journal of Basic and Applied Sciences*. 2011; 5: 295-302.

[13] Taher SA, Hemmati R, Abdolalipour A, Tabe H. Optimal decentralized load frequency control using HPSO algorithms in deregulated power systems. *American Journal of Applied Sciences*. 2008; 5(9): 1167-1174.

[14] Rao RV, Savsani VJ, Vakharia DP. Teaching-learning-based optimization: A novel method for constrained mechanical design optimization problems. *Computer-Aided Design*. 2011; 43(3): 303-315. Available from: https://doi.org/10.1016/j.cad.2010.12.015.

[15] Hassan MAM, Worku MY, Abido MA. Optimal design and real time implementation of autonomous microgrid including active load. *Energies*. 2018; 11(5): 1109. Available from: https://doi.org/10.3390/en11051109.

[16] Karimianfard H, Haghighat H, Zeng B. Co-optimization of battery storage investment and grid expansion in integrated energy systems. *IEEE Systems Journal*. 2022; 16(4): 5928-5938. Available from: https://doi.org/10.1109/JSYST.2021.3130057.

[17] Shahidehpour M, Khodayar M. Cutting campus energy costs with hierarchical control: The economical and reliable operation of a microgrid. *IEEE Electrification Magazine*. 2013; 1(1): 40-56. Available from: https://doi.org/10.1109/MELE.2013.2273994.

[18] Fayazi H, Fani B, Moazzami M, Shahgholian G. An offline three-level protection coordination scheme for distribution systems considering transient stability of synchronous distributed generation. *International Journal of Electrical Power and Energy Systems*. 2021; 131: 107069. Available from: https://doi.org/10.1016/j.ijepes.2021.107069.

[19] Hassan M, Aleem SHEA, Ali SG, Abdelaziz AY, Ribeiro PF, Ali ZM. Robust energy management and economic analysis of microgrids considering different battery characteristics. *IEEE Access*. 2020; 8: 54751-54775. Available from: https://doi.org/10.1109/ACCESS.2020.2981697.

[20] Xian S, Feng X. Meerkat optimization algorithm: A new meta-heuristic optimization algorithm for solving constrained engineering problems. *Expert Systems with Applications*. 2023; 231: 120482. Available from: https://doi.org/10.1016/j.eswa.2023.120482.

[21] Verma P, Gupta P. Proactive stabilization of grid faults in DFIG based wind farm using bridge type fault current limiter based on NMPC. *Energy Sources Part A: Recovery, Utilization, and Environmental Effects*. 2020; 45(2): 6062-6081. Available from: https://doi.org/10.1080/15567036.2019.1673508.

[22] Mohssine C, Nasser T, Essadki A. Contribution of variable speed wind turbine generator based on DFIG using ADRC and RST controllers to frequency regulation. *International Journal of Renewable Energy Research*. 2021; 11(1): 320-331.

[23] Ribó-Pérez D, Bastida-Molina P, Gómez-Navarro T, Hurtado-Pérez E. Hybrid assessment for a hybrid microgrid: A novel methodology to critically analyse generation technologies for hybrid microgrids. *Renewable Energy*. 2020; 157: 874-887. Available from: https://doi.org/10.1016/j.renene.2020.05.095.

[24] Sadat SA, Faraji J, Babaei M, Ketabi A. Techno-economic comparative study of hybrid microgrids in eight climate zones of Iran. *Energy Science and Engineering*. 2020; 8(9): 3004-3026. Available from: https://doi.org/10.1002/ese3.720.

[25] Borghei M, Ghassemi M. Optimal planning of microgrids for resilient distribution networks. *International Journal of Electrical Power and Energy Systems*. 2021; 128: 106682. Available from: https://doi.org/10.1016/j.ijepes.2020.106682.

[26] Parol M, Wójtowicz T, Księżyk K, Wenge C, Balischewski S, Arendarski B. Optimum management of power and energy in low voltage microgrids using evolutionary algorithms and energy storage. *International Journal of Electrical Power and Energy Systems*. 2020; 119: 105886. Available from: https://doi.org/10.1016/j.ijepes.2020.105886.

[27] Zhou Q, Shahidehpour M, Paaso A, Bahramirad S, Alabdulwahab A, Abusorrah A. Distributed control and communication strategies in networked microgrids. *IEEE Communications Surveys and Tutorials*. 2020; 22(4): 2586-2633. Available from: https://doi.org/10.1109/COMST.2020.3023963.

[28] Karimianfard H. A robust optimization framework for smart home energy management: Integrating photovoltaic storage, electric vehicle charging, and demand response. *Journal of Energy Storage*. 2025; 110: 115259. Available from: https://doi.org/10.1016/j.est.2024.115259.

[29] Baravati PR, Moazzami M, Hosseini SMH, Mirzaei HR, Fani B. Achieving the exact equivalent circuit of a large-scale transformer winding using an improved detailed model for partial discharge study. *International Journal of Electrical Power and Energy Systems*. 2022; 134: 107451. Available from: https://doi.org/10.1016/j.ijepes.2021.107451.

[30] Bevrani H, Habibi F, Babahajyani P, Watanabe M, Mitani Y. Intelligent Frequency Control in an AC Micro grid:Online PSO-Based Fuzzy Tuning Approach. *IEEE Transactions on Smart Grid*. 2012; 3(4): 1935-1944. Available from: https://doi.org/10.1109/TSG.2012.2196806.

[31] Li X, Song YJ, Han SB. Frequency control in micro grid power system combined with electrolyzer system and fuzzy PI controller. *Journal of Power Sources*. 2018; 180(1): 468-475. Available from: https://doi.org/10.1016/j.jpowsour.2008.01.092.

[32] Fani B, Bisheh H, Karami-Horestani A. An offline penetration-free protection scheme for PV-dominated distribution systems. *Electric Power Systems Research*. 2018; 157: 1-9. Available from: https://doi.org/10.1016/j.epsr.2017.11.020.

[33] Mauricio JM, Marano A, Gómez-Expósito A, Ramos JL. Frequency regulation contribution through variable-speed wind energy conversion systems. *IEEE Transactions on Power Systems*. 2009; 24(1): 173-180. Available from: https://doi.org/10.1109/TPWRS.2008.2009398.

[34] Morren J, De Haan SWH, Kling WL, Ferreira JA. Wind turbines emulating inertia and supporting primary frequency control. *IEEE Transactions on Power Systems*. 2006; 21(1): 433-434. Available from: https://doi.org/10.1109/TPWRS.2005.861956.

[35] Ahmadi R, Sheikholeslami A, Niaki AN, Ranjbar A. Dynamic participation of doubly fed induction generator in multi-area load frequecy control. *International Transactions on Electrical Energy Systems*. 2015; 25(7): 1130-1147. Available from: https://doi.org/10.1002/etep.1891.

[36] Karimianfard H, Salehizadeh MR, Siano P. Economic profit enhancement of a demand response aggregator through investment of large-scale energy storage systems. *CSEE Journal of Power and Energy Systems*. 2022; 8(5): 1468-1476. Available from: 10.17775/CSEEJPES.2021.02650.

[37] Li H, Wang X, Xiao J. Differential evolution-based load frequency robust control for micro-grids with energy storage systems. *Energies*. 2018; 11(7): 1686. Available from: https://doi.org/10.3390/en11071686.

[38] Stadler M, Siddiqui A, Marnay C, Aki H, Lai J. Control of greenhouse gas emissions by optimal DER technology investment and energy management in zero-net-energy buildings. *European Transactions on Electrical Power*. 2011; 21: 1291-1309. Available from: https://doi.org/10.1002/etep.418.

[39] Zhang Y, Sun Q, Zhou J, Guerrero JM, Wang R, Lashab A. Optimal frequency control for virtual synchronous generator based AC microgrids via adaptive dynamic programming. *IEEE Transactions on Smart Grid*. 2023; 14(1): 4-16. Available from: https://doi.org/10.1109/TSG.2022.3196412.

[40] Karimianfard H, Haghighat H. An initial-point strategy for optimizing distribution system reconfiguration. *Electric Power Systems Research*. 2019; 176: 105943. Available from: https://doi.org/10.1016/j.epsr.2019.105943.

[41] Heins T, Joševski M, Karthik Gurumurthy S, Monti A. Centralized model predictive control for transient frequency control in islanded inverter-based microgrids. *IEEE Transactions on Power Systems*. 2023; 38(3): 2641-2652. Available from: https://doi.org/10.1109/TPWRS.2022.3189958.

[42] Tian Z, Li X, Zha X, Tang Y, Sun P, Huang M, et al. Transient synchronization stability of an islanded ac microgrid considering interactions between grid-forming and grid-following converters. *IEEE Journal of Emerging and Selected Topics in Power Electronics*. 2023; 11(4): 4463-4476. Available from: https://doi.org/10.1109/JESTPE.2023.3271418.

[43] She B, Liu J, Qiu F, Cui H, Praisuwanna N, Wang J, et al. Systematic controller design for inverter-based microgrids with certified large-signal stability and domain of attraction. *IEEE Transactions on Smart Grid*. 2024; 15(3): 2521-2533. Available from: https://doi.org/10.1109/TSG.2023.3330705.

[44] Espín-Sarzosa D, Palma-Behnke R, Cañizares CA, Annakkage U, Elizondo M, Espina E, et al. Microgrid modeling for stability analysis. *IEEE Transactions on Smart Grid*. 2024; 15(3): 2459-2479. Available from: https://doi.org/10.1109/TSG.2023.3326063.

[45] Zhang Y, Zheng H, Zhang C, Yuan X, Xiong W, Cai Y. T-S fuzzy model based large-signal stability analysis of DC microgrid with various loads. *IEEE Access*. 2023; 11: 88087-88098. Available from: 10.1109/ACCESS.2023.3305526.

[46] Liu J, Zhang Y, Conejo AJ, Qiu F. Ensuring transient stability with guaranteed region of attraction in DC microgrids. *IEEE Transactions on Power Systems*. 2023; 38(1): 681-691. Available from: https://doi.org/10.1109/TPWRS.2022.3167315.

[47] Chen K, Baran M. Robust controller for community microgrids for stability improvement in islanded mode. *IEEE Transactions on Power Systems*. 2023; 38(3): 2472-2484. Available from: https://doi.org/10.1109/TPWRS.2022.3192459.

[48] Siano M, Parente, Ozdemir G. Resilience and stability analysis of distributed secondary controllers in DC microgrids under cyber attacks and communication delays. *IEEE Access*. 2023; 11: 132296-132311. Available from: https://doi.org/10.1109/ACCESS.2023.3335131.

[49] Ding Y, Gao F, Khan MM. Transient stability analysis of microgrid considering impact of grid-following converter's current controller. *IEEE Transactions on Power Electronics*. 2024; 39(8): 9100-9105. Available from: https://doi.org/10.1109/TPEL.2024.3395839.

[50] Liu Y, Zhang J, Liu Y, Yang M, Chen S, Zhou L, et al. An improved neural lyapunov method for transient stability assessment of networked microgrids. *IEEE Transactions on Smart Grid*. 2024; 15(2): 1410-1422. Available from: https://doi.org/10.1109/TSG.2023.3301855.

[51] Xian S, Feng X. Meerkat optimization algorithm: A new meta-heuristic optimization algorithm for solving constrained engineering problems. *Expert Systems with Applications*. 2023; 231: 120482. Available from: https://doi.org/10.1016/j.eswa.2023.120482.

[52] Abdollahzadeh B, Gharehchopogh FS, Khodadadi N, Mirjalili S. Mountain gazelle optimizer: A new nature-inspired metaheuristic algorithm for global optimization problems. *Advances in Engineering Software*. 2022; 174: 103282. Available from: https://doi.org/10.1016/j.advengsoft.2022.103282.

[53] Hussien AM, Hasanien HM, Mekhamer SF. Sunflower optimization algorithm-based optimal PI control for enhancing the performance of an autonomous operation of a microgrid. *Ain Shams Engineering Journal*. 2021; 12(2): 1883-1893. Available from: https://doi.org/10.1016/j.asej.2020.10.020.

[54] Karimianfard H, Haghighat H. Generic resource allocation in distribution grid. *IEEE Transactions on Power Systems*. 2019; 34(1): 810-813. Available from: https://doi.org/10.1109/TPWRS.2018.2867170.